small structures
www.small-structures.com

Effects of Fluorination Position on Fused-Ring Electron Acceptors

*Shuixing Dai, Jiadong Zhou, Tsz-Ki Lau, Jeromy James Rech, Kuan Liu, Peiyao Xue, Zengqi Xie, Xinhui Lu, Wei You, and Xiaowei Zhan**

Four fused-ring electron acceptors consisting of the same indacenobis(dithieno[3,2-*b*;2′,3′-*d*]thiophene) core and 2-(3-oxo-2,3-dihydroinden-1-ylidene) malononitrile end groups without or with fluorination on side chains and/or end groups are compared to probe the impacts of fluorination position on molecular packing and optical, electronic, and photovoltaic properties of the nonfullerene acceptors systematically. The fluorination on side chains blue shifts, whereas that on end groups red shifts absorption spectra. Both fluorinations downshift energy levels and enhance electron mobility. The single-crystal data show that fluorination on side chains hardly affects the aggregate structure but induces intermolecular H-bonding formation between side groups, leading to closer molecular stacking; fluorination on end groups induces formation of a larger π-orbital plane, closer framework, and interpenetrating charge-transfer pathways. While both methods of fluorinations decrease open-circuit voltage, there is an increase in short-circuit current density, fill factor, and power conversion efficiency (PCE) of organic solar cells. Finally, in combination with the polymer donor FTAZ, INIC4/INIC3 with fluorination on side chains or end groups yields PCEs of 9.6–11.6%, which is higher than INIC without fluorination (7.8%). FINIC with fluorination on both side chains and end groups yields the highest PCE of 13.0%.

1. Introduction

As a promising next-generation technology to transform renewable solar energy into clean electric energy, organic solar cells (OSCs) achieved rapid development with greatly improved performance in recent years, thanks to the concerted efforts on materials and device innovation.[1–6] Most reported high-performance OSCs are generally based on fused-ring electron acceptors (FREAs), which were pioneered by Zhan and coworkers.[7] Compared with the classical fullerene acceptors, the FREAs not only inherit advantages of fullerenes (e.g., high electron mobility) but also rectify shortcomings of fullerenes (e.g., weak absorption in visible and near-infrared regions and limited variations of frontier molecular orbital energy levels), contributing to increased power conversion efficiencies (PCEs) of OSCs.[8–34]

In 2017, we were first to report the use of fluorinated 2-(3-oxo-2,3-dihydroinden-1-ylidene)malononitrile (IC), 1FIC, and 2FIC, as electron-deficient termini in FREAs,[8] and found that the fluorination on end groups can red shift absorption spectra, down shift the frontier molecular orbitals, and enhance film crystallinity and electron mobilities. Many reported high-performance FREAs used 1FIC or 2FIC as end groups (e.g., ITIC-Th1,[12] FOIC,[14] IT-4F,[35] and Y6[36]), and the PCEs of OSCs based on fluorinated FREAs reached 17–18%.[37,38] A few works studied the effects of fluorination on end groups[8,39,40] or side chains[41] separately, but a comparison of end-group and side-chain fluorinations has not been reported.

Here, we synthesized a new fluorinated FREA based on indacenobis(dithieno[3,2-*b*;2′,3′-*d*]thiophene) (IBDT) backbone with fluorinated side chains and IC termini, namely INIC4 (**Figure 1**). Together with INIC,[8] INIC3,[8] and FINIC,[42] which were reported by our group previously, we build a small family of homologously structural FREAs with fluorination on hexylphenyl side chains, IC end groups, or both side chains

Dr. S. Dai, Dr. K. Liu, P. Xue, Prof. X. Zhan
Department of Materials Science and Engineering
College of Engineering
Key Laboratory of Polymer Chemistry and Physics of Ministry of Education
Peking University
Beijing 100871, China
E-mail: xwzhan@pku.edu.cn

Dr. S. Dai
School of Materials Science and Engineering
Ocean University of China
Qingdao 266100, China

The ORCID identification number(s) for the author(s) of this article can be found under https://doi.org/10.1002/sstr.202000006.

Dr. J. Zhou, Prof. Z. Xie
Institute of Polymer Optoelectronic Materials and Devices
State Key Laboratory of Luminescent Materials and Devices
South China University of Technology
Guangzhou 510640, China

Dr. T.-K. Lau, Prof. X. Lu
Department of Physics
The Chinese University of Hong Kong
New Territories, Hong Kong 999077, China

Dr. J. J. Rech, Prof. W. You
Department of Chemistry
University of North Carolina at Chapel Hill
Chapel Hill, NC 27599, USA

DOI: 10.1002/sstr.202000006

 © 2020 Wiley-VCH GmbH

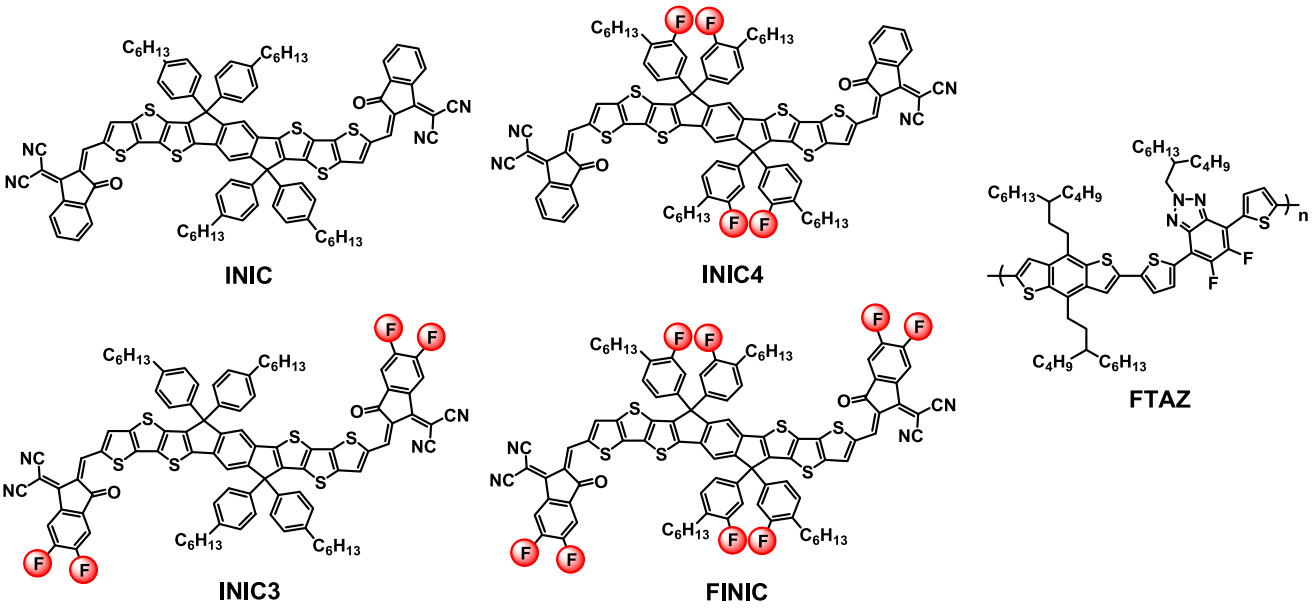

Figure 1. Chemical structures of the INIC series and FTAZ.

and end groups. We discover that fluorination on side chains leads to hypsochromic-shifted absorption spectra and enlarged optical bandgaps, whereas the fluorination on end groups results in bathochromic-shifted absorption spectra and reduced optical bandgaps. Both fluorination on side chains and end groups down shift molecular energy levels and increase electron mobilities. The single-crystal data show that the fluorination positions affect intermolecular interactions and stacking modes: the F atoms on side chains hardly affect the aggregate structure but induce intermolecular H-bonding formation between side-groups, leading to closer molecular stacking; the F atoms on end groups produce F···S interactions, leading to a larger π-orbital plane, closer framework, and interpenetrating charge-transfer pathways. OSCs based on these FREAs and our reported polymer donor FTAZ[43] (Figure 1) yield PCEs of 7.8–13.0%; the devices based on FINIC with fluorination on both side chains and end groups show the best performance.

2. Results and Discussion

2.1. Synthesis and Characterization

The synthetic route for INIC4 is shown in Scheme S1, Supporting Information, and reaction details are found in Supporting Information. All four INIC series compounds have good solubility in common organic solvents at room temperature, which is insensitive to fluorination positions. All compounds have good thermal stability with decomposition temperatures (T_d, 5% weight loss) of 311–374 °C (**Table 1** and Figure S1, Supporting Information), INIC without fluorination has the lowest T_d, while FINIC with fluorination on both side chains and end groups has the highest T_d, due to F-induced intermolecular interactions.

The absorption spectra of the INIC series are shown in **Figure 2**; their maximum molar attenuation coefficients in solutions are $2.0 - 2.5 \times 10^5$ M^{-1} cm^{-1}; their optical bandgaps (E_g) are 1.48–1.57 eV (Table 1). In thin films, all four compounds show bathochromic-shifted absorption spectra relative to their solutions. The film absorption peaks of INIC, INIC3, INIC4, and FINIC are located at 706, 744, 702, and 728 nm, respectively. Compared with that of the INIC film, the peak of INIC3 with fluorinated end groups red shifts 38 nm, the peak of INIC4 with fluorinated side chains blue shifts 4 nm, and the peak of FINIC with fluorinated side chains and end groups red shifts 22 nm. Fluorination on the side chains causes a hypsochromic shift of the absorption peak and broadening of E_g, whereas fluorination on end groups causes a bathochromic shift of the absorption peak and reduction of E_g.

The electrochemical properties of the four molecules are studied by cyclic voltammetry (CV) (Figure 2c). The lowest unoccupied

Table 1. Absorption and energy levels of the acceptors.

Compound	T_d [°C]	ε [10^5 M^{-1} cm^{-1}]	λ_{max} [nm]		E_g [eV]	HOMO [eV]	LUMO [eV]	μ_e [10^{-4} cm^2 V^{-1} s^{-1}]
			Solution	Film				
INIC	311	2.1	692	706	1.57	−5.46	−3.90	0.9
INIC3	327	2.5	710	744	1.48	−5.52	−4.00	1.7
INIC4	364	2.0	678	702	1.58	−5.50	−3.92	1.0
FINIC	374	2.4	692	728	1.51	−5.56	−4.02	8.3

© 2020 Wiley-VCH GmbH

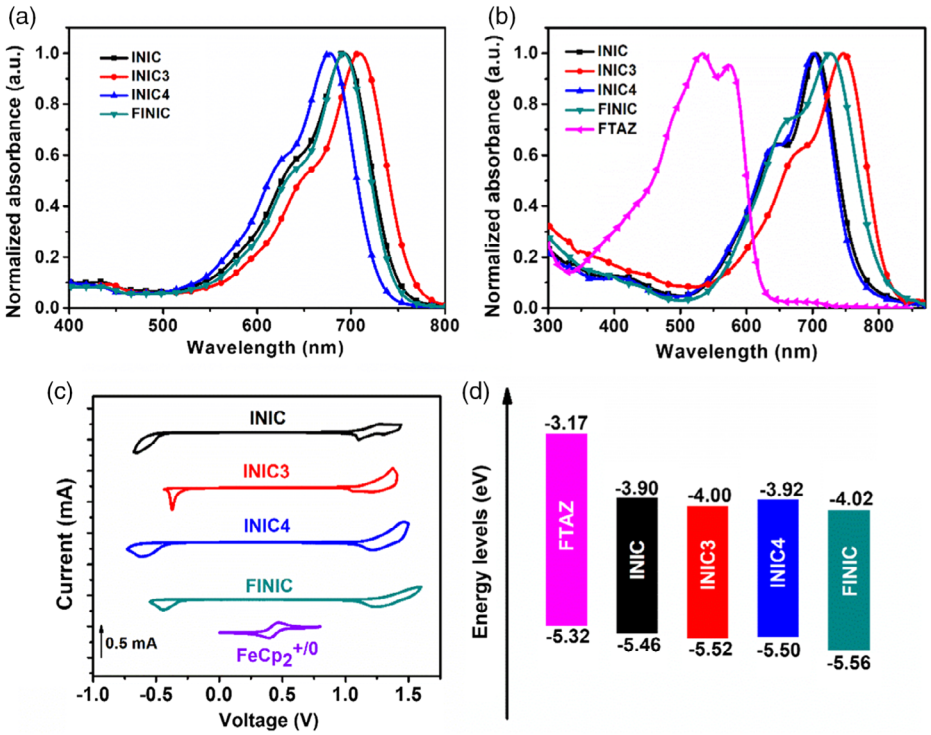

Figure 2. a) Absorption spectra of the INIC series in chloroform, b) absorption spectra of the INIC series and FTAZ as thin films, c) cyclic voltammograms of the INIC series, d) energy levels for the INIC series and FTAZ.

molecular orbital (LUMO) and highest occupied molecular orbital (HOMO) energy levels are estimated from the onset reduction and oxidation potentials, respectively (Figure 2d). The LUMO/HOMO energy levels of INIC, INIC3, INIC4, and FINIC are −3.90/−5.46, −4.00/−5.52, −3.92/−5.50, and −4.02/−5.56 eV, respectively. In comparison with those of INIC, the energy levels of INIC3 with fluorinated end groups and INIC4 with fluorinated side chains down shift, and FINIC with fluorinated end groups and side chains has the lowest energy levels. Fluorination on side chains or end groups down shifts energy levels, and the end-group fluorination has more marked influence on energy levels than the side-chain fluorination.

The electron mobilities of the INIC series compounds are measured from space charge-limited current (SCLC) with the same device structure and calculation method. The electron mobilities (μ_e) of INIC, INIC3, INIC4, and FINIC are 0.9×10^{-4},[42] 1.7×10^{-4},[8] 1.0×10^{-4}, and 8.3×10^{-4} $cm^2 V^{-1} s^{-1}$,[42] respectively (Table 1, Figure S2, Supporting Information). The fluorinated molecules have higher μ_e than the nonfluorinated INIC, and FINIC with fluorinated end groups and side chains, have the highest μ_e. This demonstrated that both fluorination on side chains and end groups is beneficial to electron transport, and end-group fluorination has a larger impact on electron transport than side-chain fluorination.

2.2. Crystallographic Analysis

The single crystals of four compounds are grown by diffusion and evaporation methods in suitable mixing solvents. The independent conformational molecules and stacking patterns are shown in **Figure 3** and crystal parameters for INIC4 and INIC3 are shown in Table S1, Supporting Information. The four compounds show planar backbones, stack into head-to-tail modes, and form 3D π–π framework.[44,45] The average π-distances of INIC, INIC3, INIC4, and FINIC are 3.33, 3.44, 3.41, and 3.40 Å, respectively (Figure S3, Supporting Information). The fluorination at different positions induces different intermolecular interactions and stacking modes. Although the F atoms on side chains hardly affect the aggregate structure due to its small spatial occupation and the rotation of phenyl rings, the intermolecular H-bonding forms between the side groups, leading to closer stacking (Figure S4, Supporting Information). On the other hand, the F atoms on terminal groups produce significant changes to the intermolecular arrangements. The F···S and O···H interactions cooperatively lead to the formation of the larger π-orbital plane, the closer framework, and interpenetrating charge-transfer pathways (Figure S4, Supporting Information).

2.3. Photovoltaic Properties

The photovoltaic properties of the INIC series were tested with an inverted structure (indium tin oxide (ITO)/ZnO/PFN-Br/FTAZ:acceptor/MoO_3/Ag). A wide-bandgap polymer FTAZ was chosen as the donor due to its complementary absorption (Figure 2b), well-aligned energy levels (Figure 2d), and a high hole mobility.[46] The optimization of devices based on FTAZ:FINIC is summarized in Supporting Information, including

© 2020 Wiley-VCH GmbH

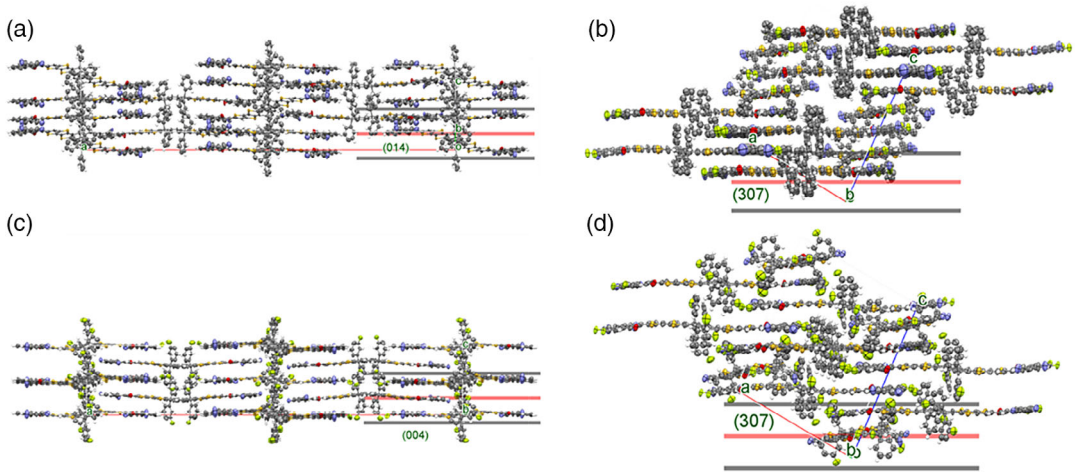

Figure 3. Oak ridge thermal-ellipsoid plot program drawing of molecular stacking patterns: a) INIC, b) INIC3, c) INIC4, and d) FINIC in the single-crystal structures. The π-planes in Miller indices are marked as red and side groups are omitted for clarity.

the donor/acceptor weight ratio (Table S2, Supporting Information) and the volume ratio of 1,8-diiodooctane (DIO) additive (Table S3, Supporting Information). All the OSCs were fabricated under optimized conditions like FTAZ:FINIC.

The current density–voltage (J–V) curves of the optimized devices based on the INIC series are shown in **Figure 4**a. The open-circuit voltages (V_{OC}) of INIC, INIC3, INIC4, and FINIC-based devices are 0.956, 0.864, 0.955, and 0.859 V, respectively (**Table 2**). The impact of fluorination on side chains and end groups leads to different trends in V_{OC}. The end-group fluorination has a negative impact on V_{OC}, as an example; when comparing INIC to INIC3, the V_{OC} decreases by ≈0.1 V upon flourination. This same decrease is found when comparing INIC4 and FINIC; this corresponds well to the CV results, which shows that LUMO decreases by ≈0.1 eV upon fluorination of the end groups. In contrast, the addition of fluorine substituents to the side chains has a minimal effect on V_{OC}, which is apparent when comparing INIC and INIC4 (0.956 vs 0.955 V). This trend also matches well with the CV data, where fluorination of the side chains maintains very close LUMO levels, examples being INIC versus INIC4 (−3.90 vs −3.92 eV) and INIC3 versus FINIC (−4.00 vs −4.02 eV).

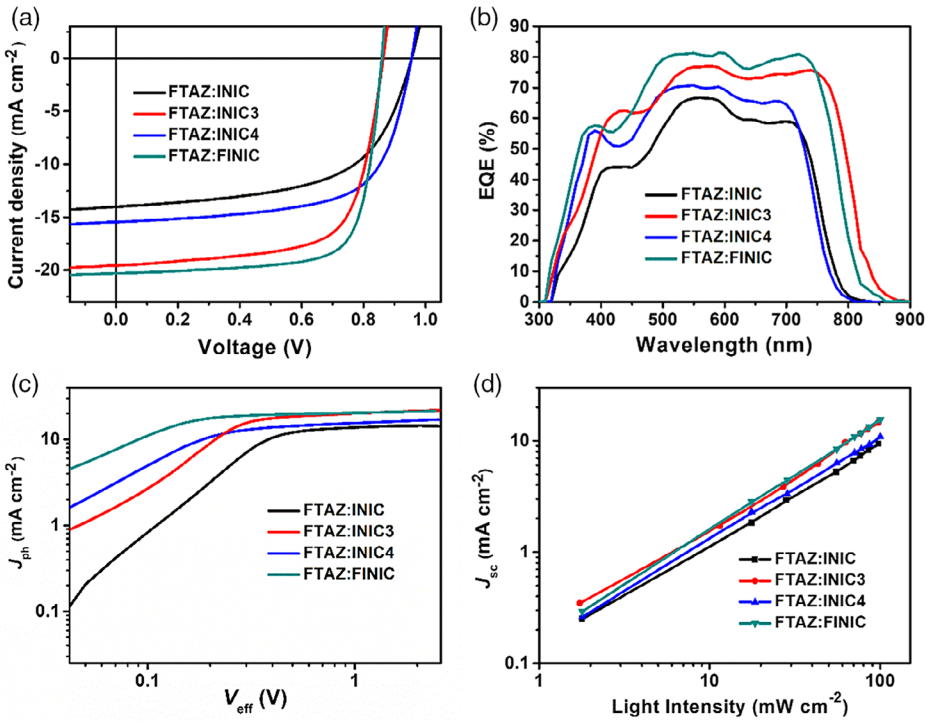

Figure 4. a) J–V characteristics and b) EQE spectra, c) J_{ph} versus V_{eff} characteristics and d) J_{SC} versus light intensity of the optimized OSCs.

© 2020 Wiley-VCH GmbH

Table 2. Performance of the Optimized OSCs.

Acceptor[a)]	V_{OC} [V]	J_{SC} [mA cm^{-2}]	Calc J_{SC} [mA cm^{-2}]	FF [%]	PCE [%]
INIC	0.961 ± 0.009 (0.956)	13.96 ± 0.05 (14.01)	13.73	55.5 ± 3.0 (58.5)	7.5 ± 0.3 (7.8)
INIC3	0.863 ± 0.009 (0.864)	20.00 ± 0.16 (19.56)	19.48	65.2 ± 3.2 (68.4)	11.3 ± 0.4 (11.6)
INIC4	0.952 ± 0.003 (0.955)	15.42 ± 0.13 (15.45)	15.05	64.9 ± 2.8 (65.0)	9.5 ± 0.2 (9.6)
FINIC	0.855 ± 0.010 (0.859)	20.35 ± 0.20 (20.31)	19.76	73.7 ± 1.0 (74.3)	12.8 ± 0.2 (13.0)

[a)]Average values with standard deviation were obtained from 20 devices and the values in parentheses are the parameters of the best device.

Short-circuit current density (J_{SC}) varies from 14.01 to 20.31 mA cm^{-2}, and a general trend of a higher J_{SC} is found when more fluorine is included on the molecule. Interestingly, the magnitude of J_{SC} impact is also dependent on the location of fluorination. When looking at the series of INIC, INIC3, and INIC4, both fluorinated acceptors have a higher J_{SC} compared with INIC; however, fluorination on the end groups (INIC3, $J_{SC} = 19.56$ mA cm^{-2}, a 40% improvement) has a larger increase than on the side chains (INIC4, $J_{SC} = 15.45$ mA cm^{-2}, a 10% improvement). This same trend is seen when comparing INIC3 with FINIC, whereas the additional side-chain fluorines only offer minor improvements in J_{SC}. This trend also makes sense in context of the absorption data, as the side-chain fluorination doesn't result in the favorable red shift that is seen with end-group fluorination. The external quantum efficiency (EQE) spectra of the OSCs are shown in Figure 4b. Similar to the aforementioned trend, fluorination results in improved values and end-group fluorination results in a larger increase than side-chain fluourination.

The fill factor (FF) varies from 58.5% to 74.3%, and a clear trend between the amount of fluorine and FF can be established. As the number of fluorine substituents increases, so does the FF value. The nonfluorinated INIC has the lowest FF of 58.5%. Adding four fluorine substituents, regardless of location on side chains or end groups, increases the FF to 65–68% (INIC3 = 68.4% and INIC4 = 65.0%). Finally, when a total of eight fluorine groups are added, the highest FF of 74.3% is found for FINIC. The charge mobilities of the blends were measured by SCLC (Figure S5 and Table S4, Supporting Information). The hole mobilities of all blends are on the same magnitude (10^{-4} cm^2 V^{-1} s^{-1}). The more fluorine, the higher μ_e, and the more balanced hole/electron mobility ratio (μ_h/μ_e), contributing to higher FF.

Finally, the improvements in J_{SC} and FF outweigh the decrease in V_{OC} which are seen upon fluroination. PCE varies from 7.8% to 13.0%. When comparing INIC3 (end-group fluorination, PCE = 11.6%) with INIC4 (side-chain fluorination, PCE = 9.6%), the large improvement in J_{SC} from end-group fluorination drives the overall higher performance. However, compared with nonfluorinated INIC (PCE = 7.8%), both methods of fluorination result in net overall improvement. In addition, by combining both side-chain and end-group fluorination methods, the highest efficiency of 13.0% is found with FINIC, primarily driven by the improved FF.

To better understand the impact of the location of fluorination, we next investigated the device physics of blends. To begin with, charge extraction was studied through the relationship of photocurrent density (J_{ph}) versus effective voltage (V_{eff}) (Figure 4c). The J_{SC}/saturation photocurrent density (J_{sat}) ratio conveys the information of charge extraction in the short-circuit condition. The J_{SC}/J_{sat} of the FINIC-based devices is 0.98, higher than those of other three devices (0.94–0.95), implying better charge extraction. Furthermore, the charge recombination was studied through the J_{SC} versus light density (P) relationship ($J_{SC} \propto P^{\alpha}$).[47] The α values of INIC-, INIC3-, INIC4-, and FINIC-based OSCs are 0.91, 0.95, 0.96, and 0.98, respectively (Figure 4d). A value of $\alpha = 1$ signifies that the blend has an insignificant bimolecular recombination. As the value of α deviated from 1, the blend has larger amounts of bimolecular recombination. This means that bimolecular recombination can be prevented by the addition of extra-fluorine substituents. From the combination of these experiments, the FINIC device has both more efficient charge extraction and less bimolecular recombination, both of which can be used to explain the superior performance.

2.4. Film Morphology

The surface morphology of the blends was measured by atomic force microscopy (AFM) (Figure S6, Supporting Information). The four blend films show smooth surfaces with root-mean-square roughness (R_q) of 0.96–1.78 nm. As the surface morphology is similar for all blends, a different approach is required to differentiate the impact of fluorination location on film morphology.

Grazing incidence wide-angle X-ray scattering (GIWAXS) measurements were used to examine the effects of fluorination position on film crystallinity and orientation.[48,49] **Figure 5** and Figure S7, Supporting Information, show 2D GIWAXS patterns and the corresponding intensity profiles of the pure and blend films. FTAZ:INIC and FTAZ:INIC4 exhibit very similar scattering patterns with the (100) lamellar peaks concentrated in the in-plane direction ($q_r \approx 0.320$ Å^{-1}, $d \approx 19.6$ Å) and the (010) π–π peaks in the out-of-plane direction ($q_z \approx 1.70$ Å^{-1}, $d \approx 3.69$ Å). It is suggested that fluorination on the side chains does not have a significant influence on molecular packing. Furthermore, the blends of acceptors with fluorinated end groups including FTAZ:INIC3 and FTAZ:FINIC also exhibit similar scattering patterns, with the lamellar peaks concentrated in the in-plane direction ($q_r \approx 0.300$ Å^{-1}, $d \approx 20.9$ Å) and the π–π peaks in the out-of-plane direction ($q_z \approx 1.75$ Å^{-1}, $d \approx 3.59$ Å). All the four blend films exhibit preferential face-on orientation. From the full width at half maximum (FWHM) of the lamellar peaks, we can estimate the crystalline correlation lengths (CCL), which are 4.1, 5.6, 4.7, and 5.4 nm for FTAZ:INIC, FTAZ:INIC3, FTAZ:INIC4, and FTAZ:FINIC, respectively. Overall, blends with acceptors

© 2020 Wiley-VCH GmbH

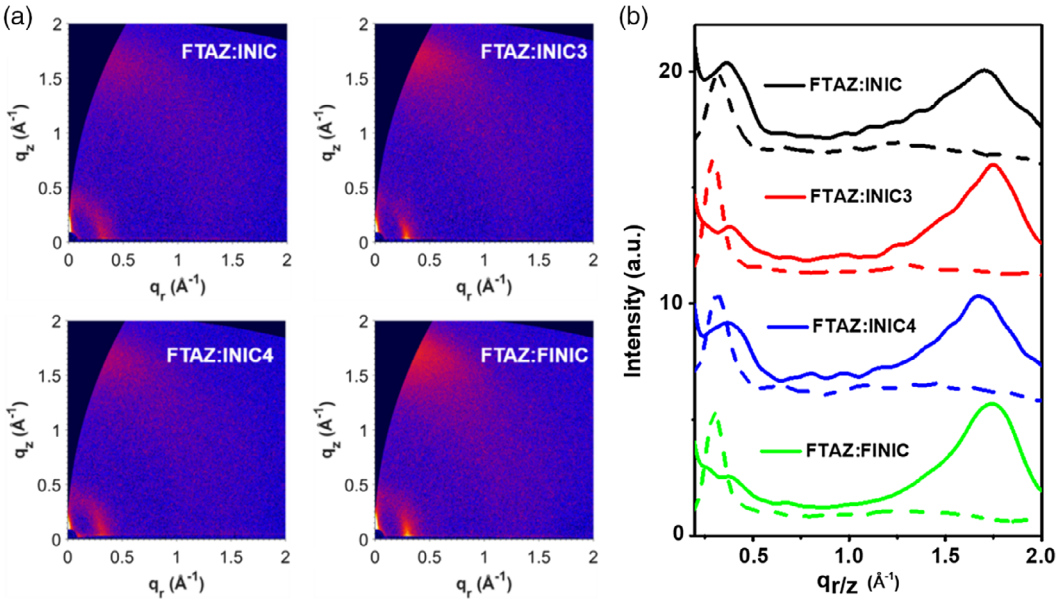

Figure 5. a) 2D GIWAXS patterns of the blend films. b) The corresponding intensity profiles in the out-of-plane (solid lines) and in-plane directions (dashed lines). All the blend films are prepared under optimized conditions (D/A = 1:1.5, w/w; 0.25% DIO, v/v).

with fluorination on the end groups show longer lamellar distances, tighter π–π stacking, and higher crystallinity, compared with those with fluorination on side chains, which will contribute to the relatively higher μ_e. The scattering intensity of FTAZ:FINIC is the highest, indicating the highest crystallinity among the four blends, in accordance with the observed highest μ_e.

In addition, GISAXS patterns of the pure and blend films are shown in Figure S8, Supporting Information, to examine the nanophase separation information. The scattering profiles of all the blend films show similar scattering features in the region of $q_r \approx 0.01$ and 0.08 $Å^{-1}$, indicative of a similar acceptor phase and FTAZ phase sizes. It implies that the more notable differences in the molecular packing measured by GIWAXS should be the more influential morphological factor related to the final device performance here.

3. Conclusion

Based on the IBDT core and various IC end groups, four INIC series compounds with/without fluorination on side chains and/or end groups were compared to study the effects of fluorination position on their crystal structure, absorption, energy levels, charge mobility, film morphology, and photovoltaic performance. The main effects of fluorination include a) fluorination on side chains causes blue shift of absorption spectrum and broadening of optical bandgap, whereas fluorination on end groups causes red shift of absorption spectrum and narrowing of optical bandgap. b) Due to the electron-withdrawing nature of fluorine atoms, fluorination on side chains or end groups down shifts energy levels, and the end-group fluorination has a more notable impact than the side-chain fluorination. c) Fluorination on side chains hardly affects the aggregate structure but induces intermolecular H-bonding formation between side groups, leading to closer molecular stacking; fluorination on end groups induces the formation of a larger π-orbital plane, closer framework, and interpenetrating charge-transfer pathways due to F···S interactions. d) Fluorination on side chains or end groups facilitates electron transport, and the end-group fluorination has a larger impact than side-chain fluorination. e) The fluorination on side chains or end groups decreases V_{OC}, but significantly increases J_{SC} and FF, eventually leading to enhanced PCE. Blends of acceptors with fluorinated end groups have higher crystallinity and tighter π–π stacking, contributing to a higher μ_e and more balanced charge transport, which is responsible for a higher J_{SC} and FF. Finally, in combination with FTAZ as the donor, INIC4/INIC3 with fluorinated side chains/end groups yields PCEs of 9.6/11.6%, higher than INIC without fluorination (7.8%). FINIC with fluorinated side chains and end groups yields the highest PCE of up to 13.0%. These results reveal that fluorination position has significant impacts on molecular packing and optoelectronic properties of the FREAs and fluorination on both side chains and end groups is a promising conception for designing high-performance nonfullerene acceptors.

Supporting Information

Supporting Information is available from the Wiley Online Library or from the author.

Acknowledgements

X.Z. thanks NSFC (No. 51761165023 and 21734001). Z.X. acknowledges the support from NSFC (51761135101 and 21733005). X.L. thanks financial support from NSFC/RGC Joint Research Scheme (grant no. N_CUHK418/17), the beam time, and technical supports provided by 23A SWAXS beamline at NSRRC. J.J.R. and W.Y. were supported by the National Science Foundation (CBET-1639429).

© 2020 Wiley-VCH GmbH

Conflict of Interest

The authors declare no conflict of interest.

Keywords

fluorination positions, fused-ring electron acceptors, nonfullerenes, organic solar cells

Received: June 18, 2020
Published online: August 14, 2020

[1] G. Li, W. H. Chang, Y. Yang, *Nat. Rev. Mater.* **2017**, *2*, 17043.
[2] G. Zhang, J. Zhao, P. C. Y. Chow, K. Jiang, J. Zhang, Z. Zhu, J. Zhang, F. Huang, H. Yan, *Chem. Rev.* **2018**, *118*, 3447.
[3] F. C. Krebs, N. Espinosa, M. Hösel, R. R. Søndergaard, M. Jørgensen, *Adv. Mater.* **2014**, *26*, 29.
[4] P. Cheng, G. Li, X. Zhan, Y. Yang, *Nat. Photonics* **2018**, *12*, 131.
[5] L. Lu, T. Zheng, Q. Wu, A. M. Schneider, D. Zhao, L. Yu, *Chem. Rev.* **2015**, *115*, 12666.
[6] C. Yan, S. Barlow, Z. Wang, H. Yan, A. K.-Y. Jen, S. R. Marder, X. Zhan, *Nat. Rev. Mater.* **2018**, *3*, 18003.
[7] Y. Lin, J. Wang, Z.-G. Zhang, H. Bai, Y. Li, D. Zhu, X. Zhan, *Adv. Mater.* **2015**, *27*, 1170.
[8] S. Dai, F. Zhao, Q. Zhang, T.-K. Lau, T. Li, K. Liu, Q. Ling, C. Wang, X. Lu, W. You, X. Zhan, *J. Am. Chem. Soc.* **2017**, *139*, 1336.
[9] S. Dai, Y. Xiao, P. Xue, J. J. Rech, K. Liu, Z. Li, X. Lu, W. You, X. Zhan, *Chem. Mater.* **2018**, *30*, 5390.
[10] S. Dai, T. Li, W. Wang, Y. Xiao, T.-K. Lau, Z. Li, K. Liu, X. Lu, X. Zhan, *Adv. Mater.* **2018**, *30*, 1706571.
[11] B. Jia, J. Wang, Y. Wu, M. Zhang, Y. Jiang, Z. Tang, T. P. Russell, X. Zhan, *J. Am. Chem. Soc.* **2019**, *141*, 19023.
[12] F. Zhao, S. Dai, Y. Wu, Q. Zhang, J. Wang, L. Jiang, Q. Ling, Z. Wei, W. Ma, W. You, C. Wang, X. Zhan, *Adv. Mater.* **2017**, *29*, 1700144.
[13] W. Wang, C. Yan, T.-K. Lau, J. Wang, K. Liu, Y. Fan, X. Lu, X. Zhan, *Adv. Mater.* **2017**, *29*, 1701308.
[14] T. Li, S. Dai, Z. Ke, L. Yang, J. Wang, C. Yan, W. Ma, X. Zhan, *Adv. Mater.* **2018**, *30*, 1705969.
[15] J. Zhu, Z. Ke, Q. Zhang, J. Wang, S. Dai, Y. Wu, Y. Xu, Y. Lin, W. Ma, W. You, X. Zhan, *Adv. Mater.* **2018**, *30*, 1704713.
[16] B. Jia, S. Dai, Z. Ke, C. Yan, W. Ma, X. Zhan, *Chem. Mater.* **2017**, *30*, 239.
[17] Z. Yao, X. Liao, K. Gao, F. Lin, X. Xu, X. Shi, L. Zuo, F. Liu, Y. Chen, A.-K. Jen, *J. Am. Chem. Soc.* **2018**, *140*, 2054.
[18] S. Li, L. Ye, W. Zhao, S. Zhang, S. Mukherjee, H. Ade, J. Hou, *Adv. Mater.* **2016**, *28*, 9423.
[19] Y. Li, J. Lin, X. Che, Y. Qu, F. Liu, L. Liao, S. R. Forrest, *J. Am. Chem. Soc.* **2017**, *139*, 17114.
[20] J. Wang, J. Zhang, Y. Xiao, T. Xiao, R. Zhu, C. Yan, Y. Fu, G. Lu, X. Lu, S. R. Marder, X. Zhan, *J. Am. Chem. Soc.* **2018**, *140*, 9140.
[21] Y. Yang, Z.-G. Zhang, H. Bin, S. Chen, L. Gao, L. Xue, C. Yang, Y. Li, *J. Am. Chem. Soc.* **2016**, *138*, 15011.
[22] Y. Zhang, B. Kan, Y. Sun, Y. Wang, R. Xia, X. Ke, Y. Q. Yi, C. Li, H. L. Yip, X. Wan, Y. Cao, Y. Chen, *Adv. Mater.* **2018**, *30*, 1707508.
[23] D. Baran, R. S. Ashraf, D. A. Hanifi, M. Abdelsamie, N. Gasparini, J. A. Rohr, S. Holliday, A. Wadsworth, S. Lockett, M. Neophytou, C. J. Emmott, J. Nelson, C. J. Brabec, A. Amassian, A. Salleo, T. Kirchartz, J. R. Durrant, I. McCulloch, *Nat. Mater.* **2017**, *16*, 363.
[24] S. Feng, C. Zhang, Y. Liu, Z. Bi, Z. Zhang, X. Xu, W. Ma, Z. Bo, *Adv. Mater.* **2017**, *29*, 1703527.
[25] X. Xu, T. Yu, Z. Bi, W. Ma, Y. Li, Q. Peng, *Adv. Mater.* **2018**, *30*, 1703973.
[26] Z. Luo, H. Bin, T. Liu, Z.-G. Zhang, Y. Yang, C. Zhong, B. Qiu, G. Li, W. Gao, D. Xie, K. Wu, Y. Sun, F. Liu, Y. Li, C. Yang, *Adv. Mater.* **2018**, *30*, 1706124.
[27] Z. Xiao, S. Yang, Z. Yang, J. Yang, H.-L. Yip, F. Zhang, F. He, T. Wang, J. Wang, Y. Yuan, H. Yang, M. Wang, L. Ding, *Adv. Mater.* **2019**, *31*, 1804790.
[28] Z. Zhou, S. Xu, J. Song, Y. Jin, Q. Yue, Y. Qian, F. Liu, F. Zhang, X. Zhu, *Nat. Energy* **2018**, *3*, 952.
[29] Y. Lin, Q. He, F. Zhao, L. Huo, J. Mai, X. Lu, C. J. Su, T. Li, J. Wang, J. Zhu, Y. Sun, C. Wang, X. Zhan, *J. Am. Chem. Soc.* **2016**, *138*, 2973.
[30] Y. Lin, F. Zhao, Q. He, L. Huo, Y. Wu, T. C. Parker, W. Ma, Y. Sun, C. Wang, D. Zhu, A. J. Heeger, S. R. Marder, X. Zhan, *J. Am. Chem. Soc.* **2016**, *138*, 4955.
[31] Y. Wu, H. Bai, Z. Wang, P. Cheng, S. Zhu, Y. Wang, W. Ma, X. Zhan, *Energy Environ. Sci.* **2015**, *8*, 3215.
[32] J. Sun, X. Ma, Z. Zhang, J. Yu, J. Zhou, X. Yin, L. Yang, R. Geng, R. Zhu, F. Zhang, W. Tang, *Adv. Mater.* **2018**, *30*, 1707150.
[33] Z. Fei, F. D. Eisner, X. Jiao, M. Azzouzi, J. A. Rohr, Y. Han, M. Shahid, A. S. R. Chesman, C. D. Easton, C. R. McNeill, T. D. Anthopoulos, J. Nelson, M. Heeney, *Adv. Mater.* **2018**, *30*, 1705209.
[34] B. B. Fan, X. Y. Du, F. Liu, W. K. Zhong, L. Ying, R. H. Xie, X. F. Tang, K. An, J. M. Xin, N. Li, W. Ma, C. J. Brabec, F. Huang, Y. Cao, *Nat. Energy* **2018**, *3*, 1051.
[35] W. Zhao, S. Li, H. Yao, S. Zhang, Y. Zhang, B. Yang, J. Hou, *J. Am. Chem. Soc.* **2017**, *139*, 7148.
[36] J. Yuan, Y. Zhang, L. Zhou, G. Zhang, H.-L. Yip, T.-K. Lau, X. Lu, C. Zhu, H. Peng, P. A. Johnson, M. Leclerc, Y. Cao, J. Ulanski, Y. Li, Y. Zou, *Joule* **2019**, *3*, 1140.
[37] Q. Liu, Y. Jiang, K. Jin, J. Qin, J. Xu, W. Li, J. Xiong, J. Liu, Z. Xiao, K. Sun, S. Yang, X. Zhang, L. Ding, *Sci. Bull.* **2020**, *65*, 272.
[38] L. Meng, Y. Zhang, X. Wan, C. Li, X. Zhang, Y. Wang, X. Ke, Z. Xiao, L. Ding, R. Xia, H.-L. Yip, Y. Cao, Y. Chen, *Science* **2018**, *361*, 1094.
[39] N. Bauer, Q. Zhang, J. J. Rech, S. Dai, Z. Peng, H. Ade, J. Wang, X. Zhan, W. You, *Nano Res.* **2019**, *12*, 2400.
[40] T. J. Aldrich, M. Matta, W. Zhu, S. M. Swick, C. L. Stern, G. C. Schatz, A. Facchetti, F. S. Melkonyan, T. J. Marks, *J. Am. Chem. Soc.* **2019**, *141*, 3274.
[41] J. Lee, E. M. Go, S. Dharmapurikar, J. Xu, S. M. Lee, M. Jeong, K. C. Lee, J. Oh, Y. Cho, C. Zhang, M. Xiao, S. K. Kwak, C. Yang, *J. Mater. Chem. A* **2019**, *7*, 18468.
[42] S. Dai, J. Zhou, S. Chandrabose, Y. Shi, G. Han, K. Chen, J. Xin, K. Liu, Z. Xie, W. Ma, Y. Yi, L. Jiang, J. Hodgkiss, X. Zhan, *Adv. Mater.* **2020**, *32*, 2000645.
[43] S. C. Price, A. C. Stuart, L. Yang, H. Zhou, W. You, *J. Am. Chem. Soc.* **2011**, *133*, 4625.
[44] J. Qu, Q. Zhang, J. Zhou, H. Lai, T. Liu, D. Li, W. Chen, Z. Xie, F. He, *Chem. Mater.* **2019**, *31*, 1664.
[45] J. Qu, D. Li, H. Wang, J. Zhou, N. Zheng, H. Lai, T. Liu, Z. Xie, F. He, *Chem. Mater.* **2019**, *31*, 8044.
[46] W. Li, S. Albrecht, L. Yang, S. Roland, J. R. Tumbleston, T. McAfee, L. Yan, M. A. Kelly, H. Ade, D. Neher, W. You, *J. Am. Chem. Soc.* **2014**, *136*, 15566.
[47] P. Schilinsky, C. Waldauf, C. J. Brabec, *Appl. Phys. Lett.* **2002**, *81*, 3885.
[48] J. Mai, T.-K. Lau, J. Li, S.-H. Peng, C.-S. Hsu, U.-S. Jeng, J. Zeng, N. Zhao, X. Xiao, X. Lu, *Chem. Mater.* **2016**, *28*, 6186.
[49] J. Mai, T.-K. Lau, T. Xiao, C.-J. Su, U. S. Jeng, N. Zhao, X. Xiao, X. Lu, *RSC Adv.* **2015**, *5*, 88500.

 © 2020 Wiley-VCH GmbH